Biochemical and *in Vivo* Characterization of a Small, Membrane-Permeant, Caspase-Activatable Far-Red Fluorescent Peptide for Imaging Apoptosis†

Kristin E. Bullok,‡ Dustin Maxwell,‡ Aparna H. Kesarwala,‡ Seth Gammon,‡ Julie L. Prior,‡ Margaret Snow,§ Sam Stanley,§ and David Piwnica-Worms*,‡,||

Molecular Imaging Center, Mallinckrodt Institute of Radiology, Department of Molecular Microbiology, and Department of Molecular Biology & Pharmacology, Washington University Medical School, St. Louis, Missouri 63110

Received September 20, 2006; Revised Manuscript Received January 12, 2007

ABSTRACT: Apoptosis is an important process involved in diverse developmental pathways, homeostasis, and response to therapy for a variety of diseases. Thus, noninvasive methods to study regulation and to monitor cell death in cells and whole animals are desired. To specifically detect apoptosis *in vivo*, a novel cell-permeable activatable caspase substrate, $TcapQ_{647}$, was synthesized and K_m, k_{cat}, and K_i values were biochemically characterized. Specific cleavage of $TcapQ_{647}$ by effector caspases was demonstrated using a panel of purified recombinant enzyme assays. Of note, caspase 3 was shown to cleave $TcapQ_{647}$ with a k_{cat} 7-fold greater than caspase 7 and 16-fold greater than caspase 6. No evidence of $TcapQ_{647}$ cleavage by initiator caspases was observed. In KB 3-1 or Jurkat cells treated with cytotoxic agents or C_6-ceramide, $TcapQ_{647}$ detected apoptosis in individual- and population-based fluorescent cell assays in an effector caspase inhibitor-specific manner. Further, only background fluorescence was observed in cells incubated with $dTcapQ_{647}$, a noncleavable all D-amino acid control peptide. Finally, *in vivo* experiments demonstrated the utility of $TcapQ_{647}$ to detect parasite-induced apoptosis in human colon xenograft and liver abscess mouse models. Thus, $TcapQ_{647}$ represents a sensitive, effector caspase-specific far-red "smart" probe to noninvasively monitor apoptosis *in vivo*.

Apoptosis is an organized, programmed cell death process by which cells are eliminated from tissues without eliciting an immune response (*1*). Biochemically, the process involves cellular detection of a death signal; protease activation for degrading organelles, critical proteins, and DNA; and the packaging of degradation products into apoptotic bodies, vesicles that are engulfed by macrophages (*2*). Visually, apoptosis leads to characteristic morphological features such as chromatin condensation, membrane ruffling, and blebbing (*2*, *3*).

Apoptosis is initiated during developmental processes, within various diseases, and upon effective chemo- and radiation therapy (*4*). Because of this, noninvasive methods to monitor the progression of apoptosis *in vivo* are desired. Successes in imaging apoptosis-related therapeutic efficacies *in vivo* have been achieved with scintigraphy and fluorescence imaging, using molecular imaging probes composed of radionuclide- or optically-labeled annexin V, as well as with MRI (*5*−*9*). Annexin V is a protein that binds phophatidylserine (PS), a phospholipid that is externalized during apoptosis. Detection of externalized PS usually correlates to apoptosis; however, false positives can occur where annexin V diffuses into necrotic, membrane-leaky cells and binds to internal PS. Another potential disadvantage of an annexin V probe is its size (36 kDa), resulting in a tendency for limited diffusion into the zones of high turgor pressure characteristic of tumor tissues (*10*). A similar approach for detecting cell death using a biotinylated C_2-domain of synaptotagmin, another PS-binding protein (*11*), has been demonstrated by labeling the domain with streptavidin-fluorescein (*11*). However, the disadvantages are similar to those of annexin V. While these techniques have provided images corresponding to cell death, such probes bind in a one-to-one ratio that potentially leads to limited signal generation. One method to improve signal generation would be use of an imaging probe employing an amplification strategy directed toward apoptosis-specific enzymes, such as the caspase (cysteinyl aspartate-specific protease) family.

Currently, 13 caspases have been identified and categorized into two main groups: initiator and effector caspases (*1*, *3*). Expressed as heterodimeric zymogens, caspases are activated by proteolytic maturation or allosteric interactions (*3*, *12*). Upon activation, caspases exclusively cleave substrates C-terminally to an aspartic acid residue. As their name implies, initiator caspases receive and transmit proapoptotic signals to effector caspases. Effector caspases then progressively degrade the cell leading to eventual cell death. Thus, activation of effector caspases generally indicates cellular commitment to apoptosis. Initiator and effector caspases are distinguished by their substrate preferences with initiator caspases (caspases 2, 8, 9, and 10) preferentially recognizing

† This work was supported by NIH Grants P50 CA94056, RO1 CA82841, and RO1 AI30084.

* Correspondence to this author at Mallinckrodt Institute of Radiology, Washington University Medical School, 510 S. Kingshighway Blvd., Box 8225, St. Louis, MO 63110. Tel: 314-362-9356. Fax: 314-362-0152. E-mail: piwnica-wormsd@mir.wustl.edu.

‡ Molecular Imaging Center, Mallinckrodt Institute of Radiology.

§ Department of Molecular Microbiology.

|| Department of Molecular Biology & Pharmacology.

10.1021/bi061959n CCC: $37.00
Published on Web 03/10/2007

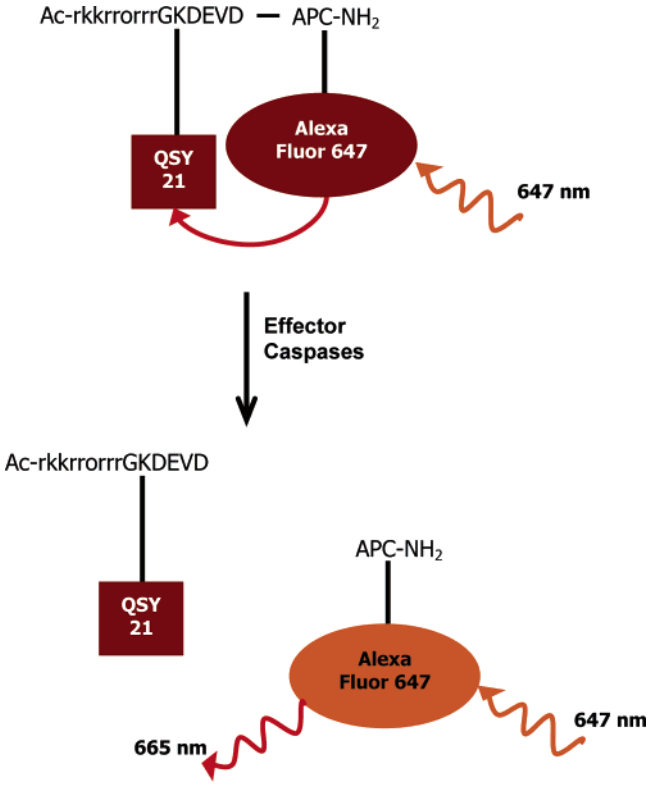

FIGURE 1: Schematic of $TcapQ_{647}$ activation following cleavage by effector caspases.

the W/HXXD sequence over the effector caspase (caspases 3, 6, and 7) recognition sequence, DXXD (*13*, *14*). These short recognition sequences have been synthesized as substrates and inhibitors to better understand caspase activity *in vitro* and *in cellulo*. Recently, the resulting tetrameric peptides have been utilized for therapeutic (*4*) and imaging purposes (*15*−*17*).

More specifically, a variety of activatable fluorescence substrates are commercially available to detect effector caspase activity. However, a majority of these substrates emit fluorescence at wavelengths that are highly absorbed by tissue (<600 nm) and, thus, are only suitable for use *in cellulo*. To design a suitable activatable effector caspase substrate for *in vivo* optical imaging of apoptosis, three main criteria should be fulfilled: fluorescence emission greater than 650 nm, low level fluorescence from the substrate in the absence of activated effector caspases, and efficient cellular internalization. One method of decreasing baseline fluorescence signal of an unactivated peptide is incorporation of an energy transfer system onto the substrate such that, upon excitation, fluorescence emission is absorbed and quenched by an adjoining nonfluorescent chromophore. Because of the low background fluorescence, a quenched fluorescence substrate, when enzymatically cleaved and activated, would provide enhanced signal and higher sensitivity for imaging target caspase activity. Thus, we designed a small imageable peptidomimetic composed of an effector caspase recognition sequence, DEVDAP, flanked by a fluorophore, Alexa Fluor 647, and a spectrally complimented quencher, QSY 21 (Figure 1). To achieve efficient and concentrative cell accumulation, an all D-amino acid permeation peptide sequence, rkkrrorrrg, was coupled to the N-terminus of the L-amino acid caspase recognition sequence. Previously, we presented the chemical synthesis and initial characterization of this cell permeable caspase substrate, $TcapQ_{647}$ (*18*). We now present detailed biochemical, cellular, and *in vivo* analysis of $TcapQ_{647}$ to demonstrate selective cleavage by effector caspases and promising applications in optical imaging of apoptosis *in vivo*.

METHODS

Preparation of Far-Red Activatable and Control Permeation Peptide Optical Probes. Peptides Ac-rkkrrorrrGK-(QSY21)DEVDAPC(AF647)-NH_2 ($TcapQ_{647}$) and Ac-rkkrrorrrgk(QSY21)devdapc(AF647)-NH_2 ($dTcapQ_{647}$) were synthesized as described (*18*). Stock solutions of purified peptides were formulated in milliQ water at various concentrations and stored at −20 °C.

Cell Culture. Cells were obtained as gifts from M. Gottesman (KB 3-1), H. Piwnica-Worms (HeLa), or S. Korsmeyer (Jurkat). Monolayers of human epidermoid carcinoma KB 3-1 and HeLa cells were grown at 37 °C in an atmosphere of 5% CO_2 as previously described (*19*, *20*). Suspensions of human Jurkat leukemia cells were maintained in RPMI also supplemented with L-glutamine, penicillin/streptomycin, and heat-inactivated fetal bovine serum at 37 °C in an atmosphere of 5% CO_2 (*21*). Monolayers of human mammary gland adenocarcinoma MCF-7 cells were grown at 37 °C in an atmosphere of 5% CO_2 in DMEM (GIBCO, Grand Island, NY) supplemented with L-glutamine (1%), penicillin/streptomycin (0.1%), and fetal bovine serum (10%) (*22*).

Fluorescence Spectrophotometric Analysis of $TcapQ_{647}$ Cleavage in Vitro. Enzyme assays were performed utilizing a fluorescence spectrophotometer (Cary Eclipse, Varian, Palo Alto, CA) with recombinant caspases 1−10 (CalBiochem, San Diego, CA) in 400 μL of caspase buffer (100 mM NaCl, 50 mM HEPES, 10 mM DTT, 1 mM EDTA, 10% glycerol, and 0.1% CHAPS, pH 7.4) or a modified caspase buffer (50 mM NaCl, 50 mM HEPES, 10 mM DTT, 1 mM EDTA, 5% glycerol, and 0.1% CHAPS, pH 7.4; caspase 2) at 37 °C. Assays utilized 5 U each of the caspases. Note that one U caspase 3 activity equals 1.0 pmol of substrate cleavage per min per μg of enzyme, while one U caspase activity for all others equals 1.0 nmol of substrate cleavage per h per mg of enzyme. Enzymes were preincubated in buffer briefly (caspase 8 and 9) or for 30 min (remaining caspases) before initiation of the assay by addition of $TcapQ_{647}$ (1 μM, final concentration) to the enzyme solutions in a cuvette. Similar experiments were performed with recombinant granzyme B and cathepsin B (CalBiochem, San Diego, CA). Increases in fluorescence were monitored over time with measurements recorded every 20 s using a 5 nm slit width at 647 nm (excitation) and a 10 nm slit width at 670 nm (emission). The photomultiplier tube voltage was set to medium (600 V). Background fluorescence of $TcapQ_{647}$, as determined in the absence of enzyme, was subtracted from raw fluorescence units. Subsequently, initial apparent cleavage rates were determined by fitting the linear regime of the time−activity curve for each enzyme.

Kinetic Analysis of $TcapQ_{647}$ Cleavage. At least two independent caspase inhibition assays were performed for each effector caspase. Recombinant effector caspases (0.13 nM caspase 3, 6.6 nM caspase 6, 3.1 nM caspase 7) were

preincubated at 37 °C in 400 μL of caspase buffer with increasing concentrations of the inhibitor, DEVD-CHO (Calbiochem, La Jolla, CA), for 40 min. Assays were initiated by addition of $TcapQ_{647}$ or SubII (DEVD-AMC, Calbiochem, La Jolla, CA) at final concentrations of 0.5 μM (caspase 6 and 7 assays) or 1 μM (caspase 3 assay). Increases in fluorescence were monitored at 37 °C using spectrophotometric settings identical to above. Initial rates were determined by curve fitting the linear regime and were plotted against inhibitor concentration. EC_{50} values were determined by nonlinear regression analysis. Using the experimentally derived EC_{50} values and validated (SubII) or published K_i values, the apparent K_m ($TcapQ_{647}$) for each enzyme was calculated based upon the Cheng−Pruschoff relationship: $EC_{50} = K_i(1 + [S]/K_m)$, where [S] is the concentration of substrate (*23*). Apparent k_{cat} values were calculated using the equation $k_{cat} = V(K_m+[S])/[E][S]$, where V is the initial rate of cleavage, [S] is the concentration of substrate, and [E] is the concentration of enzyme (*24*).

Confocal Microscopy. KB 3-1 cells (6×10^5) were plated in a 35 mm glass coverslip dish in full media as noted above. Media was removed 24 h later, and cells were pretreated with fresh media containing 5 μM doxorubicin for 13−15 h. HeLa and MCF-7 cells were similarly pretreated. Before peptide addition, pretreatment media was removed and cells were washed with modified Earl's balanced salt solution (MEBSS; composed of (mM) 145 Na^+, 5.4 K^+, 1.2 Ca^{2+}, 0.8 Mg^{2+}, 152 Cl^-, 0.8 $H_2PO_4^-$, 0.8 SO_4^{2-}, 5.6 dextrose, 4.0 HEPES, and 1% heat-inactivated fetal bovine serum (vol/vol), pH 7.4) at 37 °C. Peptides, either $TcapQ_{647}$ or $dTcapQ_{647}$ (4 μM, final concentration) and (L-aspartate)$_2$-rhodamine 110 (D_2R, 5 μM, final concentration; Biotium, Hayward, CA) in MEBSS were then added to the cells for a 20 min incubation at 37 °C. Finally, propidium iodide (PI; 3 μL of a 1 mg/mL stock solution) was added post-peptide incubation. Coincubation of cells with the general caspase substrate, D_2R, confirmed the presence of apoptotic cells; propidium iodide was added to document cell membrane integrity. In the presence of peptide, cells were analyzed for fluorescence activation by live-cell confocal microscopy (slice thickness of 11 μM) using an inverted Zeiss Axiovert 200 laser scanning confocal microscope coupled to a Zeiss LSM 5 PASCAL fitted with excitation lasers at 488 nm (for D_2R), 543 nm (for PI), 633 nm (for $TcapQ_{647}$) and bandpass emission filters of 505−530 nm (for D_2R) and 560−615 nm (for PI) as well as a long-pass emission filter of 650 nm (for $TcapQ_{647}$). For analysis, at least 4 fields at 40× magnification were examined and scored for apoptotic cells. The presence of cytoplasmic fluorescence was scored positive for apoptosis. Occasional focal punctuate fluorescence was not scored.

Fluorescence Spectrophotometric Analysis of $TcapQ_{647}$ Activation: Dose−Response in Jurkat Cells. Exponentially growing Jurkat cells were collected by centrifugation (1200 rpm) and resuspended in fresh, full media to 5×10^5 cells/mL. For each condition, 1 mL aliquots were plated in 35 mm dishes and incubated for 45−60 min before addition of vehicle (DMSO) or C_6-ceramide (BIOMOL International, Plymouth Meeting, PA; 5−80 μM). For inhibition studies, cells were first pretreated with the caspase 3 inhibitor, D(OMe)QMD(OMe)-FMK (40 μM) (Calbiochem, La Jolla, CA), for 1 h before addition of C_6-ceramide (40 μM). Following a 3 h C_6-ceramide treatment, cells were pelleted as before and resuspended in 500 μL of MEBSS at 37 °C. Cells were transferred to a cuvette maintained at 37 °C for fluorometric analysis. The assay was initiated upon addition of $TcapQ_{647}$ (4 μM, final concentration), and fluorescence increases over time were continuously monitored over 20 min using 5 nm (excitation) and 10 nm (emission) slit widths with excitation at 645 nm and emission at 670 nm. The photomultiplier tube voltage was set to medium (600 V). Following fluorometric analysis of each condition, cell suspensions were immediately placed at −80 °C until Western blot analysis. Cell viability at each ceramide concentration was determined in tandem with fluorescence assays. Following a 3 h treatment with the appropriate C_6-ceramide concentration, 3 aliquots of $\sim 1.5 \times 10^5$ cells (based on pretreatment cell density) were removed from each condition, pelleted, resuspended in fresh media, and transferred to a 96-well plate (60 μL per well). An equal volume (60 μL per well) of WST-1 cell proliferation reagent (Roche; Indianapolis, IN) diluted (1:5) in media was then added to each well, and the plate was incubated at 37 °C with 5% CO_2 for 70 min. Viability was determined by measuring absorption at 450 nm minus absorption at 750 nm. Values were plotted as percent viability and were used to normalize fluorescence data.

Western Blot Analysis. Jurkat cells obtained from each condition of the concentration−response study above and stored at −80 °C were analyzed for activation of caspase 3. Cells were thawed on ice and pelleted (1200 rpm). Cell pellets were resuspended in hypotonic lysis buffer (10 mM KCl, 1.5 mM $MgCl_2$, 10 mM Tris-HCl, 1% SDS, pH 7.4, supplemented with 10 μg/mL leupeptin, 10 μg/mL aprotinin, and 0.5 mM PMSF) and sonicated on ice. Approximately equal amounts of protein from whole-cell lysates were loaded into each lane of a 15% polyacrylamide gel prior to electrophoresis. Following transfer of protein to an Immobilon-P PVDF membrane (Millipore, Billerica, MA), blots were probed with a rabbit polyclonal antibody against procaspase 3 (1:100; Santa Cruz Biotechnology, Santa Cruz, CA). Blots were then stripped and reprobed with rabbit anti-β-actin antibody (1:100; Sigma-Aldrich, St Louis, MO) to normalize for loading. Immune complexes were detected by probing blots with horseradish peroxidase-conjugated anti-rabbit secondary antibody (1:1000; Amersham, Piscataway, NJ) and enhanced chemiluminescence reagent (Amersham, Piscataway, NJ) prior to imaging with a cooled CCD camera (IVIS 100 system, Xenogen, Alameda, CA; open filter, f-stop 1, binning 4, 2−3 min exposure). Band intensity was analyzed using Living Image/Igor Pro 2.5 software.

Colon-Xenograft and Liver Mouse Model of Entamoeba histolytica Infection. Animal protocols were approved by the Animal Studies Committee at Washington University School of Medicine. To establish a bilateral human colon xenograft mouse model, human colonic xenografts were placed into the subscapular region of 6−8 week old SCID or SCID/beige mice as previously described (*25*). Incisions were closed with Michel clips. Xenografts were allowed to develop for 8−10 weeks before use, at which time the clips were removed. The mice were fed an alfalfa-free diet 5 days before imaging, and their fur was removed using a depilating powder 1 day before imaging. Left colonic xenografts were then infected by direct intraluminal inoculation with 1×10^6 *E. histolytica* trophozoites (strain HM1:IMSS) grown on BI-

S-33 as previously described (*26*). Right xenografts were mock-infected with media to serve as controls. For the liver parasite-induced abscess model, livers of SCID mice were surgically exposed and infected in a single lobe with 1×10^6 *E. histolytica* trophozoites (strain HM1:IMSS). Abscesses were allowed to form for 24 h in both mouse models. A total of 12 mice with colonic xenografts were analyzed as follows: following i.p. injection of $TcapQ_{647}$ (0.1 mg/1.5 mL saline, $n = 6$), $dTcapQ_{647}$ (0.1 mg /1.5 mL saline, $n = 4$), or saline vehicle (1.5 mL, $n = 2$), mice were imaged at 0, 30, 60, and 90 min postinjection on a Kodak Multimodality Image Station 4000MM using a 625/670 nm excitation/emission filter set and a CCD camera (binning 4×4). X-ray images were obtained and overlaid with corresponding fluorescence images. Xenografts were removed and images were again obtained using similar settings. All fluorescence images were normalized to the footpad and then compared to those from saline-only injected mice. Xenografts were then fixed in 10% formalin overnight and then kept in 70% EtOH before embedding in paraffin. Representative slices of colonic tissue (4 μm thick) were then imaged by confocal microscopy using an inverted Zeiss Axiovert 200 laser scanning confocal microscope coupled to a Zeiss LSM 5 PASCAL and analyzed for cell death by TUNEL staining (Washington University Digestive Disease Research Core). Samples were semiquantified as null (zero staining), + (scattered staining), ++ (moderate staining), and +++ (abundant staining) ($TcapQ_{647}$ xenografts, $n = 4$; $dTcapQ_{647}$ xenografts, $n = 2$; and saline vehicle xenograft, $n = 1$). For liver experiments ($n = 3$), peptide and saline solutions were i.p. injected as above and mice were euthanized 90 min postinjection. Livers were immediately removed and imaged using the identical settings described above. For image analysis of $TcapQ_{647}$ activation, mean fluorescence intensity was determined by drawing regions of interest around each xenograft and liver lobe using Kodak 4000MM 1D imaging software. All *in vivo* images were normalized as a ratio of the infected graft to the background autofluorescence from each animal. *Ex vivo* images of infected and mock-infected grafts were normalized to saline injected grafts.

Analysis. Data were reported as mean values ± standard error of the mean (SEM). Pairs were compared with the Student *t* test (*27*), and values of $P \leq 0.05$ were considered significant. For rank-order analysis, the Spearman correlation coefficient, r_s, was calculated to compare data sets.

RESULTS

Chemical synthesis and spectral characterization of $TcapQ_{647}$ was described in detail (*18*). Briefly, a greater than 92% quenching efficiency was determined for both the hydrolyzable peptide, $TcapQ_{647}$, and the nonhydrolyzable all D-amino acid peptide, $dTcapQ_{647}$, in water, in cellular media, and in 100% serum. Absorption spectrometry analysis of the intact peptides revealed a blue-shifted absorption maximum and indicated that fluorescence quenching occurred through a mechanism other than classical Förster resonance energy transfer. Previous initial recombinant enzyme assays indicated that $TcapQ_{647}$ was preferentially cleaved by effector caspases 3 and 7 over initiator caspase 9. This was expected as the DEVD sequence is generally thought to be recognized more efficiently by effector caspases than by initiator caspases (*13*). To further characterize $TcapQ_{647}$ cleavage by the caspase family, enzymatic proteolysis of $TcapQ_{647}$ by a full panel of recombinant caspases was examined.

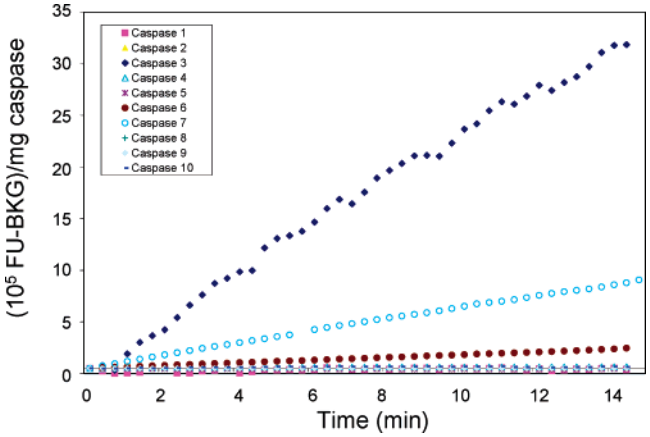

FIGURE 2: Recombinant enzyme assays demonstrating the selectivity of $TcapQ_{647}$ cleavage by effector caspases. Assays were performed with equal units of activity (5 U) and normalized to mg of caspase for each enzyme. $TcapQ_{647}$ cleavage rates were highest for the effector caspases 3, 7, and 6. Assays with initiator and inflammatory caspases resulted in slow cleavage rates, with most initiator caspases demonstrating no proteolytic activity toward $TcapQ_{647}$. FU represents arbitrary fluorescence units.

Recombinant caspase assays were performed using continuous fluorometric analysis. To determine and compare the initial rates of $TcapQ_{647}$ cleavage by each of the caspases 1−10, identical units of enzyme activity (5 U) were utilized and results normalized to mg of enzyme (Figure 2). Rates of $TcapQ_{647}$ cleavage were determined by linear curve fit. As can be seen, caspase 3 cleaved $TcapQ_{647}$ at a much greater rate than the other effector caspases with an initial cleavage rate over background of 2.2×10^5 FU min^{-1} mg^{-1}, while caspase 7 and caspase 6 cleaved $TcapQ_{647}$ at 0.59×10^5 FU min^{-1} mg^{-1} and 0.14×10^5 FU min^{-1} mg^{-1}, respectively. Little to no cleavage of $TcapQ_{647}$ was observed upon incubation with any of the initiator caspases. To confirm the lack of proteolysis, units of enzyme activity were increased to 20 U and 50 U (data not shown) and assays were performed as above. $TcapQ_{647}$ cleavage by initiator caspases was minimal (0.002×10^5 FU min^{-1} mg^{-1}) as observed by fluorometry at these higher caspase protease concentrations. These data indicated that $TcapQ_{647}$ was preferentially cleaved by effector caspases. Confirming probe specificity, no detectable increase in fluorescence was observed upon incubation of $TcapQ_{647}$ with two other proteases, granzyme B and cathepsin B, that are also implicated in cell death processes (data not shown).

To fully characterize the kinetics of $TcapQ_{647}$ cleavage, the apparent K_m and k_{cat} values for caspases 3, 6, and 7 were determined. An indirect method for determining the apparent K_m values was necessary due to the extensive inner-filter effect observed in cuvettes with $TcapQ_{647}$, even at low (submicromolar) concentrations. Thus, to avoid analytical complications due to the inner-filter effect, inhibition assays using the inhibitor, DEVD-CHO, were performed to derive EC_{50} values and subsequently calculate the apparent K_m values for each effector caspase using the Cheng−Prushoff relationship (Methods). By using the same $TcapQ_{647}$ concentration for each assay, the loss of fluorescence intensity due to the inner-filter effect remains constant for each experiment.

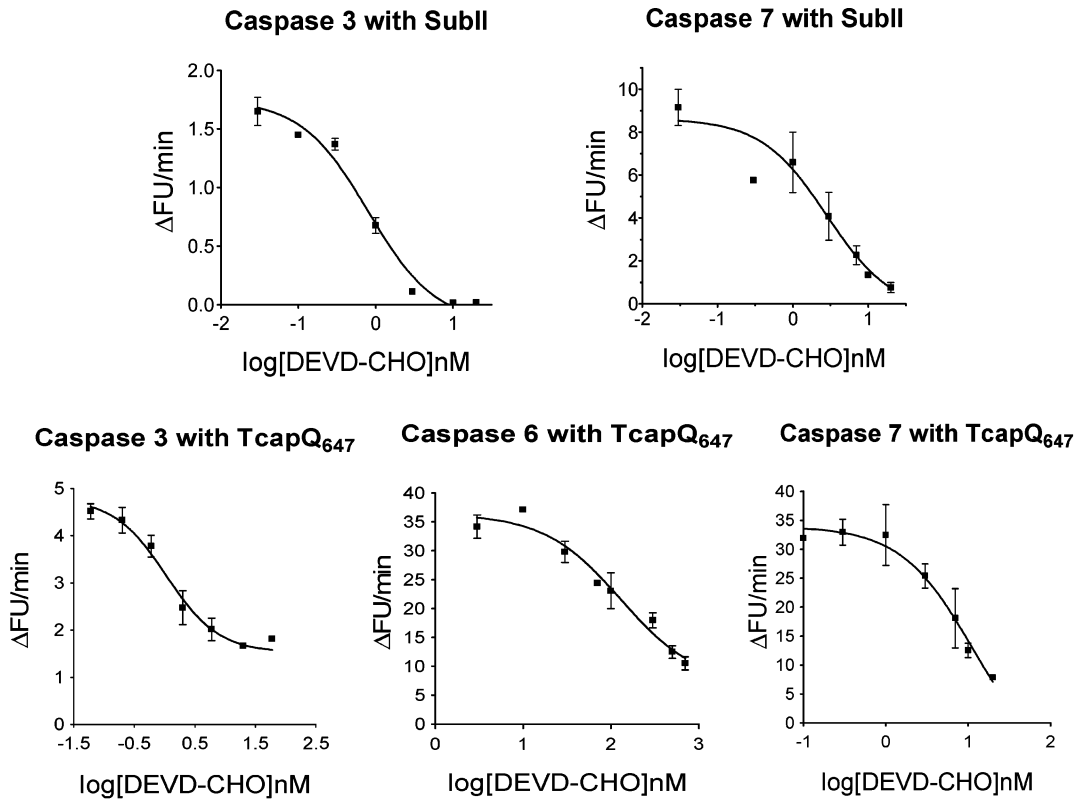

FIGURE 3: Inhibition curves of executioner caspases. Caspases were incubated with increasing concentrations of the reversible caspase inhibitor, DEVD-CHO, before addition of the substrate SubII (0.5 μM, for caspase 7; 1 μM, for caspase 3) or TcapQ$_{647}$ (0.5 μM, for caspase 6 and 7; 1 μM, for caspase 3). EC_{50} values were determined from rates of fluorescence increase (ΔFU min^{-1}) using nonlinear regression analysis and were utilized to calculate K_i values for DEVD-CHO (using SubII) or K_m values for TcapQ$_{647}$. Bars indicate SEM.

To validate such an inhibition assay, a caspase 7 inhibition assay was performed using the inhibitor, DEVD-CHO, to confirm the published $K_{i,cas7}$ value (1.6 nM) (*28*, *29*). Three independent inhibition curves were generated using the commercial fluorescent substrate, DEVD-AMC (SubII). For each assay, caspase 7 was preincubated with increasing concentrations of the inhibitor, DEVD-CHO and the assay initiated by addition of SubII (0.5 μM, final concentration). At each inhibitor concentration, the apparent rate of fluorescence increase was determined using linear curve fit data and the average rates of fluorescence increase from each independent experiment were plotted against inhibitor concentration (Figure 3). Nonlinear regression analysis was then utilized to fit these data and determine the EC_{50} value. Using the Cheng−Prushoff relationship (*23*), the experimentally determined EC_{50} value and the published $K_{m,cas7}$ value (11 μM) (*30*) were used to calculate a SubII-derived apparent $K_{i,cas7}$ value for DEVD-CHO of 1.4 nM. This is in good agreement with the published $K_{i,cas7}$ value (1.6 nM), thus validating the use of this inhibition assay to determine kinetic parameters of TcapQ$_{647}$ cleavage by caspases. Similarly, a second control experiment was performed to determine which $K_{i,cas3}$ value within the published range (0.23−2.3 nM) (*28*, *29*) would be appropriate for use in the present caspase 3 inhibition study. Caspase 3 was preincubated with the inhibitor, DEVD-CHO, before initiation of the assay by addition of SubII (1 μM, final concentration). Three independent assays were carried out, and the rate of fluorescence increase for each condition was averaged as above (Figure 3). The EC_{50} value, as determined by nonlinear regression analysis, was utilized with the published K_m value (10 μM) (*30*) to calculate a SubII-derived apparent $K_{i,cas3}$ value for DEVD-CHO of 0.73 nM. This value is well within the published range of $K_{i,cas3}$ values and was employed in the inhibition assays below to calculate the K_m of TcapQ$_{647}$ cleavage by caspase 3.

Table 1: Kinetic Parameters of TcapQ$_{647}$ Cleavage

caspase	EC_{50} (nM)	K_i (nM)	K_m (nM)	"k_{cat}" (FU min^{-1} μM^{-1})	"k_{cat}/K_m" (FU min^{-1} μM^{-1})/nM)
3	1.2	0.73	1500	89000	6.0×10^1
7	11	1.4	73	13000	1.8×10^2
6	130	31[a]	160	5700	3.6×10^1

[a] Published value.

At least two independent inhibition assays for each effector caspase (caspases 3, 6, and 7) were then carried out as above to determine the kinetics of TcapQ$_{647}$ cleavage by each effector caspase. From the averaged rate data, inhibition curves were generated to determine the EC_{50} values for each enzyme (Figure 3) and to calculate apparent K_m and k_{cat} values. The rank order of preferential cleavage of TcapQ$_{647}$ was caspase 3 > caspase 7 > caspase 6 as determined from the apparent k_{cat} values (Table 1).

Upon establishing the kinetics of TcapQ$_{647}$ cleavage by effector caspases, we determined the utility of TcapQ$_{647}$ to detect the presence of apoptosis in individual living cells using confocal microscopy. For these studies, adherent KB 3-1 cells were grown on 35 mm glass-bottom microwell dishes. Cells remained untreated or treated with doxorubicin (5 μM), a drug which has been shown to induce apoptosis via caspase activation (*31*). After treatment, cells were

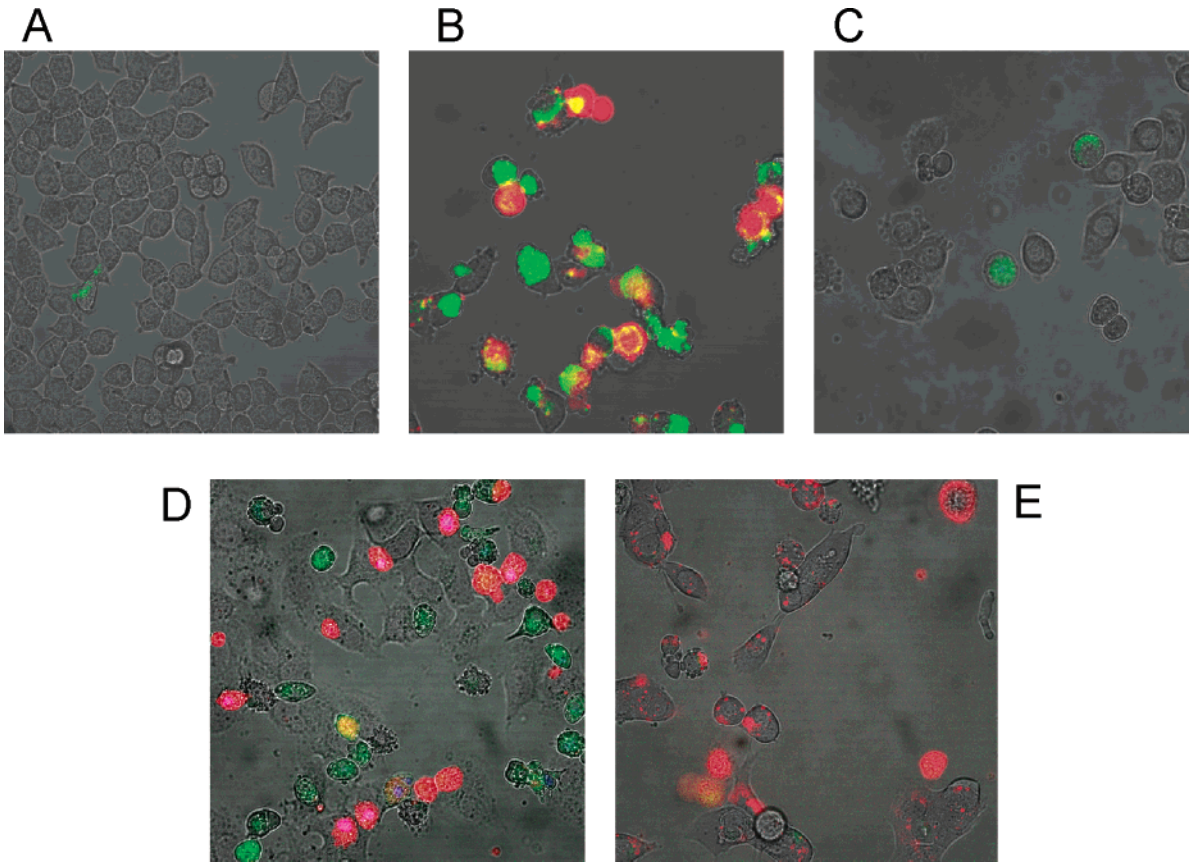

FIGURE 4: Intracellular activation of $TcapQ_{647}$ during apoptosis. (A) Untreated KB 3-1 cells incubated with $TcapQ_{647}$, bis (L-aspartate) rhodamine 110 (D_2R), and PI. (B) Doxorubicin-treated (5 μM) KB 3-1 cells incubated with $TcapQ_{647}$, D_2R, and PI. (C) Doxorubicin-treated KB 3-1 cells incubated with noncleavable $dTcapQ_{647}$, D_2R, and PI. (D) Doxorubicin-treated HeLa cells incubated with $TcapQ_{647}$, D_2R, and PI. (E) Doxorubicin-treated MCF-7 cells incubated with $TcapQ_{647}$, D_2R, and PI. Red fluorescence indicates activation of $TcapQ_{647}$, green fluorescence indicates activation of D_2R, yellow fluorescence indicates colocalization of D_2R with $TcapQ_{647}$, and purple indicates colocalization of PI with $TcapQ_{647}$.

simultaneously incubated with $TcapQ_{647}$ (4 μM) and a commercial quenched fluorescence caspase substrate, bis-aspartate rhodamine (D_2R; 5 μM). For control experiments, cells were incubated with the nonhydrolyzable all D-amino acid peptide, $dTcapQ_{647}$, along with D_2R. For all conditions, propidium iodide was added to the cells prior to confocal microscopy analysis. D_2R activation was observed as green fluorescence, while $TcapQ_{647}$ activation was observed as red fluorescence. PI staining of membrane-compromised cells was falsely colored as blue fluorescence for ease of overlay analysis. As can be seen, $TcapQ_{647}$ activation was observed in doxorubicin treated cells but not in untreated cells (Figure 4). Colocalization of D_2R and $TcapQ_{647}$ activation was also observed (Figure 4B; yellow cells). As compared to $TcapQ_{647}$, a larger number of cells demonstrated D_2R activation, consistent with its utility as a general caspase substrate, while $TcapQ_{647}$ is a specific effector caspase substrate. Cells positive for both $TcapQ_{647}$ activation and PI staining were also observed (Figure 4B, purple cells). Control studies with noncleavable $dTcapQ_{647}$ resulted in low fluorescence background, indicating that the observed fluorescence in cells incubated with $TcapQ_{647}$ was due to enzymatic proteolysis rather than conformational change of the quenched peptide (Figure 4C). Previous inhibition studies (*18*) support these results and demonstrated that $TcapQ_{647}$ activation was inhibited upon treatment of cells with the effector caspase inhibitor, D(OMe)QMD(OMe)-FMK. $TcapQ_{647}$ activation was further demonstrated in two other cell lines (HeLa, MCF-7) treated with doxorubicin (Figure 4D,E), indicating the general applicability of the imaging probe.

We next determined the utility of $TcapQ_{647}$ to detect increasing apoptosis in a cell population following treatment of cells with increasing concentrations of drug. For this concentration−response assay, Jurkat cells were utilized as they are a well-established apoptotic cell model and are grown in suspension. Induction of apoptosis by C_6-ceramide has been well characterized in Jurkat cells (*32*, *33*). Thus, apoptosis was induced in the Jurkat cell population by incubation with increasing concentrations of C_6-ceramide as described (Methods).

In Jurkat cells, the rate of $TcapQ_{647}$ activation increased proportionately with ceramide concentrations (Figure 5A). These observations correlated with decreases in cell viability as measured by MTS assay (Figure 5B). Treatment with greater than 30 μM C_6-ceramide resulted in substantial decreases in cell viability as observed both by endpoint MTS analysis (Figure 5B) and phase contrast microscopy (data not shown). No increase in fluorescence was observed when Jurkat cells were incubated with the noncleavable control peptide, $dTcapQ_{647}$ (data not shown). Finally, $TcapQ_{647}$ activation was completely abrogated in cells pretreated with the effector caspase inhibitor D(OMe)QMD(OMe)-FMK (Figure 5C). These data indicated that the extent of $TcapQ_{647}$ activation was proportional to the amount of apoptosis occurring in a given cell population.

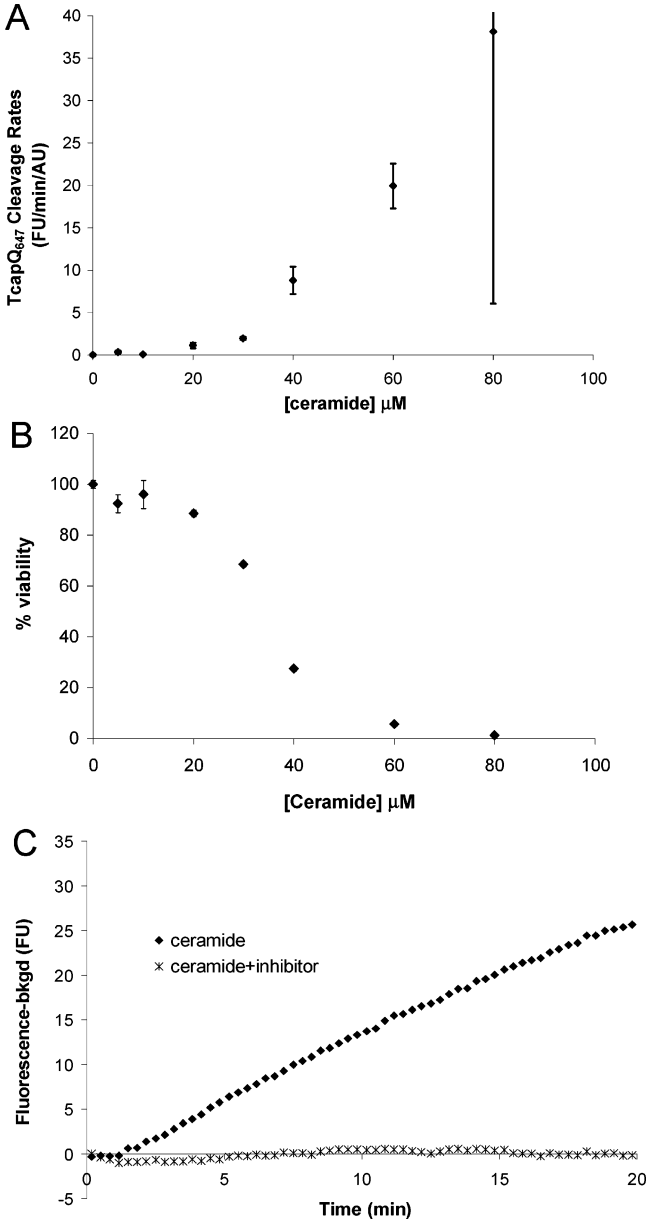

FIGURE 5: Jurkat cell concentration−response assay as determined by $TcapQ_{647}$ activation. Jurkat cells were treated with increasing concentrations of C_6-ceramide for 3 h to induce apoptosis, and then incubated with $TcapQ_{647}$, and increases in fluorescence were monitored over time. (A) Initial rates of $TcapQ_{647}$ cleavage were normalized to cell viability and plotted against concentration of C_6-ceramide. AU represents absorption units from MTS analysis, and FU represents fluorescence units. (B) Viability of Jurkat cells as determined by MTS analysis following treatment of cells with increasing concentration of C_6-ceramide. (C) Analysis of $TcapQ_{647}$ activation in C_6-ceramide-treated (40 μM) Jurkat cells with or without the caspase inhibitor D(OMe)QMD(OMe)-FMK (40 μM). Bars indicate SEM.

To independently confirm activation of caspase 3 in the ceramide-treated Jurkat cells, Western blot analysis of each condition from the above assay was performed. As shown, the amount of procaspase 3 decreased with increasing concentrations of C_6-ceramide (Figure 6A), indicating activation of caspase 3. Western blot analysis of procaspase 3 was normalized to total protein in each lane as determined by β-actin levels. Normalized data were plotted against C_6-ceramide concentration (Figure 6B) to determine the concentration−response of procaspase 3 activation. The approximate EC_{50} value (15 μM) of C_6-ceramide-induced proteolysis of procaspase 3 correlated with the concentration of C_6-ceramide where activation of $TcapQ_{647}$ was first observed via analysis by fluorescence spectrophotometry (Figure 5A).

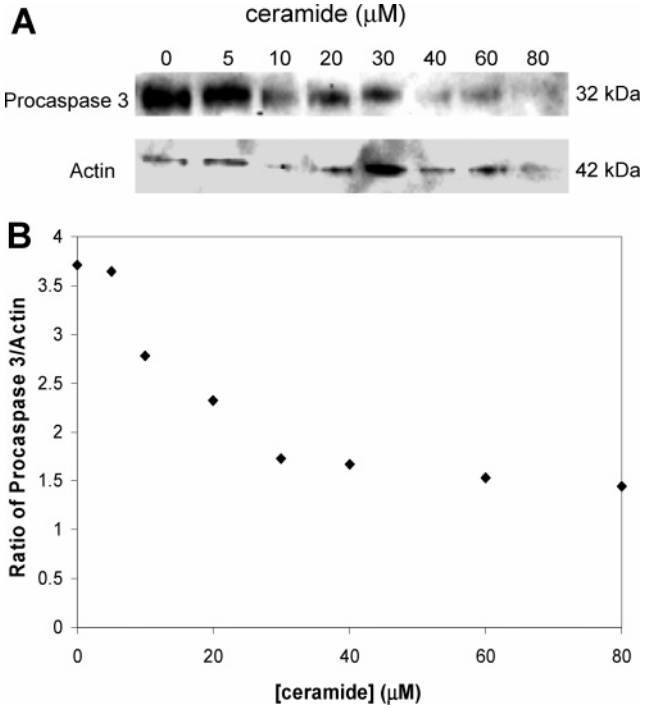

FIGURE 6: Western blot of Jurkat cell lysates following treatment for 3 h with increasing concentrations of C_6-ceramide. (A) The blot was probed with anti-procaspase 3 antibody to monitor decreases in the level of procaspase 3 following treatment with C_6-ceramide. To normalize the level of procaspase 3 in each lane, the blot was stripped and reprobed with anti-β-actin antibody. (B) Ratio of procaspase 3 levels to β-actin levels as determined by Western blot analysis plotted against increasing concentrations of C_6-ceramide.

To determine the utility of $TcapQ_{647}$ to detect apoptosis *in vivo*, two *E. histolytica*-infected mouse models were utilized. The first model involved a human colon xenograft mouse model where sections of human colonic tissue were grafted into the subscapular region of SCID or SCID/beige mice (*25*). Once established, xenografts were infected with amoeba trophozoites by direct intraluminal injection. At 4 h postinjection, damage to the host intestinal lining can be observed (*25*). Tissue destruction following infection with *E. histolytica* has been associated with apoptosis (*34*). Because of the surface location of the xenografts, this mouse model seemed ideal for initial examination of *in vivo* activation of $TcapQ_{647}$ in tissues undergoing apoptosis. The second model involved direct injection of *E. histolytica* into a single lobe of the liver and subsequent local abscess formation or use of saline as a control.

For colon experiments *in vivo*, mice with bilateral xenografts were utilized. The region around the xenografts was shaved and depilated prior to infecting the left xenograft with *E. histolytica* and the right xenograft with parasite-free media as a control. For colon xenograft experiments 24 h postinfection, mice were imaged over time following i.p. injection of either $TcapQ_{647}$ (0.1 mg/ 1.5 mL saline), noncleavable $dTcapQ_{647}$ (0.1 mg/ 1.5 mL saline), or saline (Figure 7). Colon xenografts were then removed and imaged *ex vivo*, and representative samples were subsequently analyzed by

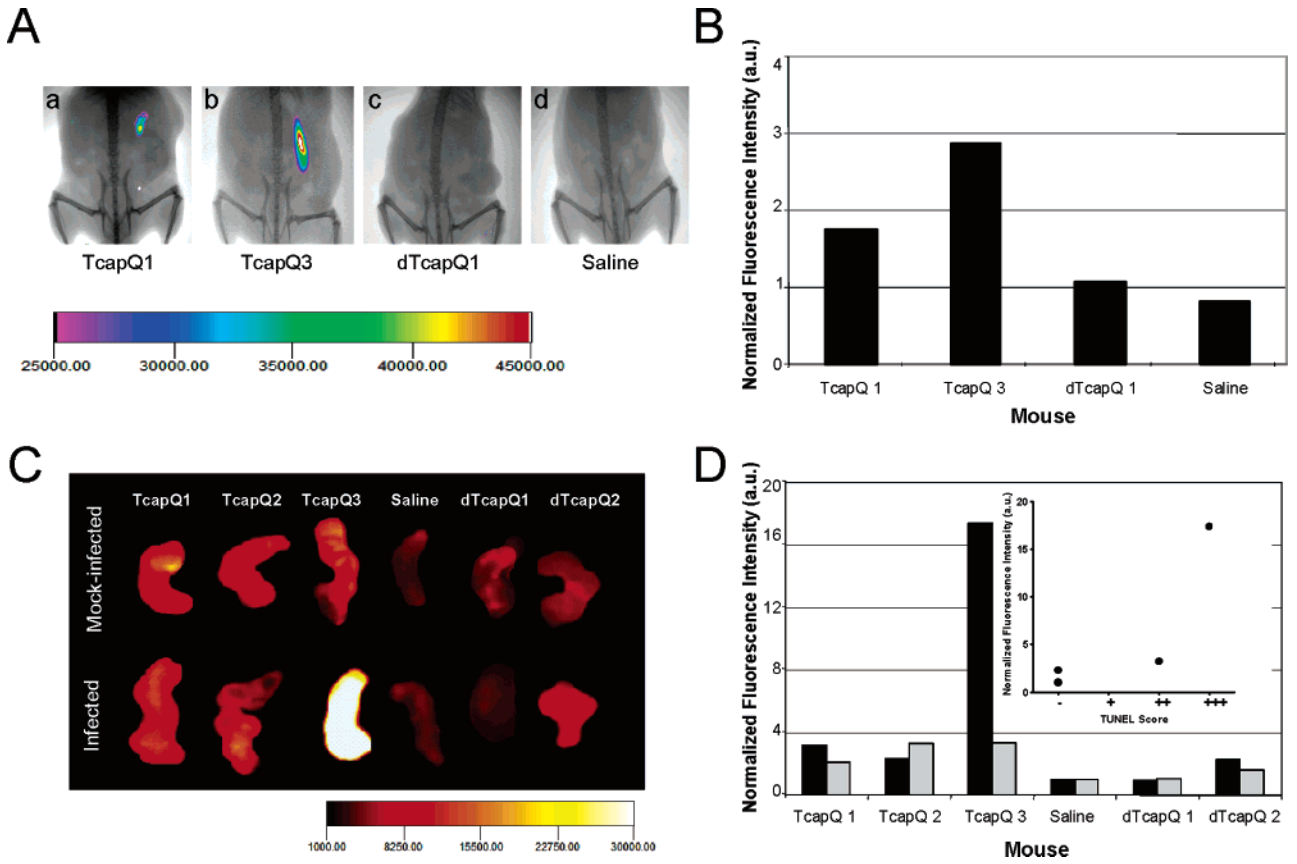

FIGURE 7: Far-red fluorescence images of colonic xenograft in mice *in vivo*. Human colonic xenografts were mock-infected as a control or infected with *E. histolytica* 24 h prior to i.p. injection of $TcapQ_{647}$ ($n = 6$), noncleavable $dTcapQ_{647}$ ($n = 4$), or saline ($n = 2$). (A) Representative fluorescence images of mice with bilateral xenografts 60 min postinjection of the indicated solution. The mock-infected xenograft is located in the left half of each image (mouse right side) whereas the amoeba-infected xenograft is located in the right half of each image. Fluorescence and X-ray images were obtained on a Kodak Multimodality Imaging Station 4000MM. Images are falsely colored and overlaid with corresponding X-ray images. (B) Graphical representation of the normalized fluorescence intensity of *in vivo* xenograft images as determined by region of interest analysis. Assigned numerals following TcapQ or dTcapQ indicate individual mice. (C) Fluorescence images of *ex vivo* xenografts comparing fluorescence intensity in mock- and amoeba-infected xenografts corresponding to several mice in (A). (D) Graphical representation of the normalized fluorescence intensity of *ex vivo* xenograft images as determined by region of interest analysis of *ex vivo* images. Assigned numerals following TcapQ or dTcapQ indicate individual mice. Black bars, amoeba-infected xenograft; gray bars, mock-infected xenograft. Inset: Correlation of normalized $TcapQ_{647}$ fluorescence intensity for amoeba-infected xenografts and TUNEL score.

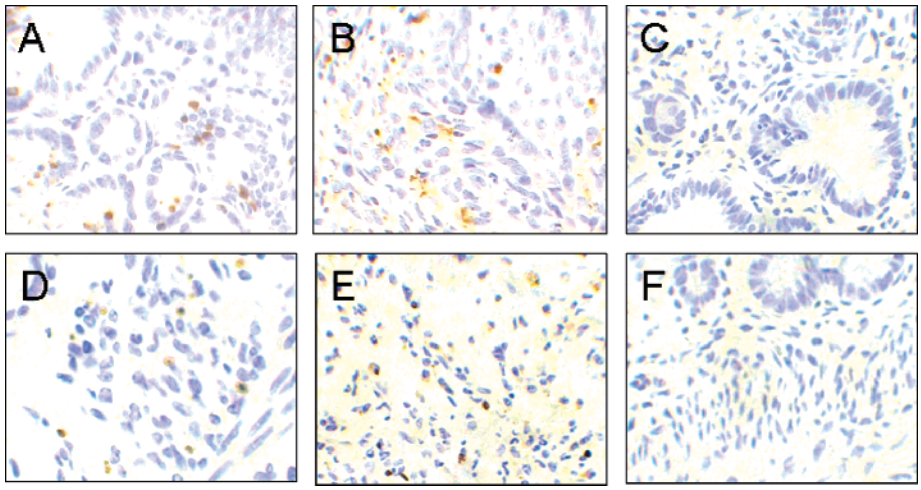

FIGURE 8: TUNEL analysis of grafts from colon xenograft mouse model comparing mock- and amoeba-infected tissues. (A) Positive control for TUNEL stain. (B) Amoeba-infected xenograft from TcapQ3. (C) Mock-infected xenograft from mouse TcapQ3. (D) Amoeba-infected xenograft from TcapQ1. (E) Amoeba-infected xenograft from noncleavable dTcapQ1. (F) Amoeba-infected xenograft from dTcapQ2. All images were obtained using a 40× objective on a Zeiss Axiovert 200 laser scanning confocal microscope. Assigned numerals following TcapQ or dTcapQ indicate individual mice.

TUNEL staining (Figure 8). Overall, images *ex vivo* correlated with images *in vivo* (Figure 7A,C). Apoptosis by TUNEL staining was surprisingly variable in amoeba-infected xenografts, being present only in selected specimens

Table 2: Mean Fluorescence Intensity of *ex Vivo* Liver Lobes[a]

condition	infected	mock
liver, $TcapQ_{647}$	6000	3700
liver, saline	500	*

[a] Livers were infected with *E. histolytica* or mock-infected as a control. * indicates not assessed. Mean fluorescence intensity was determined by ROI analysis of the entire lobe using Kodak Multimodality Imaging Station 4000MM 1D imaging software.

(e.g., Figure 8B,D,E,F), but not observed, as expected, in mock-infected xenografts (e.g., Figure 8C). Region of interest (ROI) analysis of $TcapQ_{647}$ signal in colon xenografts (Figure 7C) correlated with the presence of apoptosis as determined by TUNEL analysis (Figure 8B−D). For example, the amoeba-infected xenograft of mouse TcapQ3 resulted in the highest fluorescence signal (5-fold greater than the background observed in the corresponding mock-infected xenograft) and also showed the highest TUNEL signal. A similar, but less dramatic result was observed in the mouse TcapQ1 (Figure 7A−D). Analysis of mouse TcapQ2, which had been infected, but showed no detectable fluorescence signal, also showed no positive TUNEL staining in the amoeba-infected xenograft. For mice injected with the noncleavable peptide $dTcapQ_{647}$, little (dTcapQ2) to no (dTcapQ1) fluorescence was observed in all amoeba-infected relative to mock-infected xenografts (Figure 7). TUNEL analysis confirmed the presence of apoptosis in the dTcapQ1 amoeba-infected xenograft, but not in the dTcapQ2 amoeba-infected xenograft (Figure 8E,F). Overall, for those samples analyzed by both methods, activation of $TcapQ_{647}$ *in vivo* correlated with the presence of apoptosis as determined by TUNEL staining (Figure 7D, inset; $r_s = 0.948$, $n = 4$), while background signal from $dTcapQ_{647}$ did not. Similar increases in fluorescence over controls were observed with *ex vivo* analysis of liver lobes using the parasitic liver mouse model (Table 2). Thus, the extent of $TcapQ_{647}$ activation *in vivo* appeared to be indicative of the level of apoptosis present in a given tissue.

DISCUSSION

This study presented full biochemical and *in vivo* characterization of a permeation peptide-based imaging substrate specific for effector caspases. These kinetic studies indicate that $TcapQ_{647}$ is strongly and preferentially cleaved by effector caspases over initiator caspases. Furthermore, in contrast to our pilot data suggesting similar kinetics for caspases 3 and 7 (*18*), full analysis for $TcapQ_{647}$ showed k_{cat} values of 89 000, 13 000, and 5700 FU min^{-1} μM^{-1} for caspase 3, caspase 7, and caspase 6, respectively, indicating preferential cleavage of $TcapQ_{647}$ by caspase 3. Of note, caspase 3 cleaved $TcapQ_{647}$ at an absolute rate greater than the commercial substrates MCA-DEVDAP-DNP (SubIII; data not shown) and DEVD-AMC (SubII). Similarly, caspase 7 was observed to cleave $TcapQ_{647}$ at a greater rate than SubII.

The differences between $TcapQ_{647}$ and commercial substrates are the size of the chromophore(s), the length of the peptide sequence, and the mechanism of fluorescence quenching, any of which could impact overall kinetics. Previous studies by others showed that SubII was cleaved by caspases 3 and 7 with identical K_m values near 11 μM (*13*, *30*). The K_m of $TcapQ_{647}$ toward 3 and 7 were in the low μM to nM range, respectively, which would be advantageous for imaging *in vivo* since substrate concentrations would likely be present within these molar ranges. Interestingly, kinetic studies herein demonstrated that caspase 3 cleaved $TcapQ_{647}$ with an apparent k_{cat} 7-fold greater than caspase 7, which is almost identical to k_{cat} ratios for substrates reported by Thornberry et al. Thus, $TcapQ_{647}$ exhibited similar biochemical properties to other probes already studied, but also provided certain affinity advantages for detecting caspases 3 and 7 in the *in vivo* setting.

Absorption spectrometry analysis indicated that $TcapQ_{647}$ fluorescence was not quenched via a classical Förster resonance energy transfer (FRET). Instead, the absorption maximum of the $TcapQ_{647}$ fluorophore, Alexa Fluor 647, was blue-shifted from 650 nm in the absence of the quencher, QSY 21, to 605 nm in the presence of the quencher, indicating the presence of a strong Coulombic interaction between the transition dipole moments of QSY 21 and Alexa Fluor 647 (*35*). The altered spectrum is thought to arise when such a chromophore interaction leads to the formation of an intramolecular dimer called an exciton (*36*) and a subsequent split in excitation energy levels (*37*). Depending on the electronics of the dimer, the absorption spectrum can either be blue-shifted, called an H-dimer, where radiative transitions to the lower excitation level are forbidden, or red-shifted, called a J-dimer, where radiative transitions to the higher excitation level are forbidden (*35*, *38*, *39*). Such interactions have been shown to impose secondary structure to peptide sequences positioned between chromophores (*39*). Taken together, these spectral and kinetic data indicate that flanking effector caspase recognition sequences with exciton-forming chromophores may impact specific conformational states, kinetics, and specificity of the peptide sequences.

With respect to whole cell assays, $TcapQ_{647}$ was shown to be efficiently and specifically activated by caspases *in cellulo*. $TcapQ_{647}$ activation was demonstrated by confocal microscopy to correlate with cleavage of the general caspase substrate, D_2R, on an individual KB 3-1 cell basis. In population-based fluorometric analysis, $TcapQ_{647}$ activation was shown to increase proportionately with the increases in ceramide-induced Jurkat cell death. As would be expected, the observed $TcapQ_{647}$ activation signals were effectively attenuated upon treatment of cells with an effector caspase inhibitor. In contrast, no increase in fluorescence intensity was observed in cells upon incubation with the all D-amino acid noncleavable peptide, $dTcapQ_{647}$, on either an individual or population-based analysis.

Finally, this study demonstrated the utility of $TcapQ_{647}$ in detecting amoeba-induced cell death *in vivo*. In mice with bilateral colon xenografts, a greater increase in fluorescence intensity was observed in *E. histolytica*-infected over mock-infected xenografts following $TcapQ_{647}$ injection. In contrast, no significant increase in fluorescence intensity was observed following injection with the noncleavable peptide, $dTcapQ_{647}$. Similar data were observed in the amoeba-infected liver lobes over mock-infected liver lobes. The extent of this $TcapQ_{647}$ activation in amoeba-infected xenografts varied from animal to animal. However, TUNEL analysis of excised colonic tissue indicated that this was due to varying levels of cell death within each xenograft. Importantly, a strong positive correlation ($r_s = 0.948$) was observed between the amount

of TUNEL stain and the level of $TcapQ_{647}$ activation. In contrast, little to no increase in fluorescence intensity was observed following injection with the noncleavable peptide, $dTcapQ_{647}$, even in TUNEL positive tissue.

In conclusion, this study demonstrated favorable properties of $TcapQ_{647}$ to detect apoptosis in cultured cells and *in vivo*. The incorporation of a quenched fluorescence strategy onto the cell-permeable caspase substrate resulted in little to no detectable fluorescence signal in the absence of activated caspases. By utilizing a far-red fluorophore, caspase cleavage resulted in light emission above 650 nm, where intrinsic photon absorption by cells and tissues is low. Further, the chosen quencher−fluorophore pair, QSY 21/Alexa Fluor 647, generated an enzyme substrate highly specific for effector caspases. Finally, $TcapQ_{647}$ activation was shown to correlate with cellular activation of caspase 3 and with *ex vivo* analysis of cell death via TUNEL staining. Modifications to the TcapQ scaffold could provide a panel of compounds with altered protease specificity and further improvements in light penetration from activation in deep tissues.

ACKNOWLEDGMENT

Special thanks to Vijay Sharma and Samuel Achilefu for valuable discussions, the Hope Center for Neurological Diseases at Washington University for confocal microscopy use, and the Washington University Digestive Diseases Research Core Center for tissue preparation and TUNEL staining.

REFERENCES

1. Grutter, M. (2000) Caspases: key players in programmed cell death, *Curr. Opin. Struct. Biol. 10*, 649−655.
2. Shi, Y. (2001) A structural view of mitochondria-mediated apoptosis, *Nat. Struct. Biol. 8*, 394−401.
3. Kroemer, G., and Martin, S. (2005) Caspase-independent cell death, *Nat. Med. 11*, 725−730.
4. Fischer, U., and Schulze-Osthoff, K. (2005) New approaches and therapeutics targeting apoptosis in disease, *Pharmacol. Rev. 57*, 187−215.
5. Ran, S., and Thorpe, P. E. (2002) Phosphatidylserine is a marker of tumor vasculature and a potential target for cancer imaging and therapy, *Int. J. Radiat. Oncol. Biol. Phys. 54*, 1479−1484.
6. Van De Wiele, C., Lahorte, C., Vermeersch, H., Loose, D., Mervillie, K., Steinmetz, N., Vanderheyden, J., Cuvelier, C., Slegers, G., and Dierck, R. (2003) Quantitative tumor apoptosis imaging using technetium-99m HYNIC annexin V single photon emission computed tomography, *J. Clin. Oncol. 21*, 3483−3487.
7. Petrovsky, A., Schellenberger, E., Josephson, L., Weissleder, R., and Bogdanov, A. J. (2003) Near-infrared fluorescent imaging of tumor apoptosis, *Cancer Res. 63*, 1936−1942.
8. Schellenberger, E., Bogdanov, A. J., Petrovsky, A., Ntziachristos, V., Weissleder, R., and Josephson, L. (2003) Optical imaging of apoptosis as a biomarker of tumor response to chemotherapy, *Neoplasia 5*, 187−192.
9. Hamstra, D., Chenevert, T., Moffat, B., Johnson, T., Meyer, C., Mukherji, S., Quint, D., Gebarski, S., Fan, X., Tsien, C., Lawrence, T., Junck, L., Rehemtulla, A., and Ross, B. (2005) Evaluation of the functional diffusion map as an early biomarker of time-to-progression and overall survival in high-grade glioma, *Proc. Natl. Acad. Sci. U.S.A. 102*, 16759−16764.
10. Jain, R. (2005) Normalization of tumor vasculature: an emerging concept in antiangiogenic therapy, *Science 307*, 58−62.
11. Jung, H., Kettunen, M., Davletov, B., and Brindle, K. (2004) Detection of apoptosis using the C2A domain of synaptotagmin I, *Bioconjugate Chem. 15*, 983−987.
12. Riedl, S., and Shi, Y. (2004) Molecular mechanisms of caspase regulation during apoptosis, *Nat. Rev. Mol. Cell Biol. 5*, 897−906.
13. Thornberry, N. A. (1997) A combinatorial approach defines specificities of members of the caspase family and granzyme B, *J. Biol. Chem. 272*, 17907−17912.
14. Lien, S., Pastor, R., Sutherlin, R., and Lowman, H. (2004) A substrate-phage approach for investigating caspase specificity, *Protein J. 23*, 413−425.
15. Smolewski, P., Bedner, E., Du, L., Hsieh, T. C., Wu, J. M., Phelps, D. J., and Darzynkiewicz, Z. (2001) Detection of caspases activation by fluorochrome-labeled inhibitors: Multiparameter analysis by laser scanning cytometry, *Cytometry 44*, 73−82.
16. Komoriya, A., Packard, B. Z., Brown, M. J., Wu, M. L., and Henkart, P. A. (2000) Assessment of caspase activities in intact apoptotic thymocytes using cell-permeable fluorogenic caspase substrates, *J. Exp. Med. 191*, 1819−28.
17. Zhang, H.-Z., Kasibhatla, S., Guastella, J., Tseng, B., Drewe, J., and Cai, S. X. (2003) N-Ac-DEVD-N′-(Polyfluorobenzoyl)-R110: Novel cell-permeable fluorogenic caspase substrates for the detection of caspase activity and apoptosis, *Bioconjugate Chem. 14*, 458−463.
18. Bullok, K., and Piwnica-Worms, D. (2005) Synthesis and characterization of a small, membrane-permeant, caspase-activatable far-red fluorescent peptide for imaging apoptosis, *J. Med. Chem. 48*, 5404−5407.
19. Akiyama, S. I., Fojo, A., Hanover, J. A., Pastan, I., and Gottesman, M. M. (1985) Isolation and genetic characterization of human KB cell lines resistant to multiple drugs, *Somatic Cell Mol. Genet. 11*, 117−126.
20. Piwnica-Worms, D., Chiu, M., Budding, M., Kronauge, J., Kramer, R., and Croop, J. (1993) Functional imaging of multidrug-resistant P-glycoprotein with an organotechnetium complex, *Cancer Res. 53*, 977−984.
21. Polyakov, V., Sharma, V., Dahlheimer, J., Pica, C., Luker, G., and Piwnica-Worms, D. (2000) Novel Tat-peptide chelates for direct transduction of technetium-99m and rhenium into human cells for imaging and radiotherapy, *Bioconjugate Chem. 11*, 762−771.
22. Luker, G. D., Flagg, T. P., Sha, Q., Luker, K. E., Pica, C. M., Nichols, C. G., and Piwnica-Worms, D. (2001) MDR1 P-glycoprotein reduces influx of substrates without affecting membrane potential, *J. Biol. Chem. 276*, 49053−49060.
23. Burlingham, B. T., and Widlanski, T. S. (2003) An intuitive look at the relationship of Ki and IC50: a more general use for the Dixon Plot, *J. Chem. Educ. 80*, 214−218.
24. Mathews, C., van Holde, K., and Ahern, K. (2000) *Biochemistry*, 3rd ed., Benjamin Cummings, San Francisco.
25. Zhang, Z., Wang, L., Seydel, K., Li, E., Ankri, S., Mirelman, D., and Stanley, S. (2000) Entamoeba histolytica cysteine proteinases with interleukin-1 beta converting enzyme (ICE) activty cause intestinal inflammation and tissue damage in amoebiasis, *Mol. Microbiol. 37*, 542−548.
26. Stanley, S. J., Becker, A., Kunz-Jenkins, C., Foster, L., and Li, E. (1990) Cloning and expression of a membrane antigen of Entamoeba histolytica possessing multiple tandem repeats, *Proc. Natl. Acad. Sci. U.S.A. 87*, 4976−4980.
27. Glantz, S. A. (1987) *Primer of Biostatistics*, 2nd ed., p 379, McGraw-Hill, Inc., New York.
28. Salgado, J., Garcia-saez, A., Malet, G., Mingarro, I., and Perez-Paya, E. (2002) Peptide in apoptosis research, *J. Pept. Sci. 8*, 543−560.
29. Ekert, P., Silke, J., and Vaux, D. (1999) Caspase inhibitors, *Cell Death Differ. 6*, 1081−1086.
30. Talanian, R. V., Quinlan, C., Trautz, S., Hackett, M. C., Mankovich, J. A., Banach, D., Ghayur, T., Brady, K. D., and Wong, W. W. (1997) Substrate specificities of caspase family proteases, *J. Biol. Chem. 272*, 9677−9682.
31. Dimanche-Boitrel, M., Meurette, O., Rebillard, A., and Lacour, S. (2005) Role of early plasma membrane events in chemotherapy-induced cell death, *Drug Resist. Updates 8*, 5−14.
32. Herr, I., Wilhelm, D., Bohler, T., Angel, P., and Debatin, K.-M. (1997) Activation of CD95 (APO-1/Fas) signaling by ceramide mediates cancer therapy-induced apoptosis, *EMBO J. 16*, 6200−6208.
33. Lin, C., Chen, C., Chang, W., Jan, M., Hsu, L., Wu, R., Tang, M., Chang, W., and Lin, Y. (2004) Sequential caspase-2 and

caspase-8 activation upstream of mitochondria during ceramide and etoposide-induced apoptosis, *J. Biol. Chem. 279*, 40755−40761.
34. Huston, C., Boettner, D., Miller-Sims, V., and Petri, W. J. (2003) Apoptotic killing and phagocytosis of host cells by the parasite *Entamoeba histolytica*, *Infect. Immun. 71*, 964−972.
35. Kasha, M. (1963) Energy transfer mechanism and molecular exciton model for molecular aggregates, *Radiat. Res. 20*, 55−71.
36. Hernando, J., van der Schaaf, M., van Dijk, E., Sauer, M., Garcia-Parajo, M., and van Hulst, N. (2003) Excitonic behavior of rhodamine dimers: a single-molecule study, *J. Phys. Chem. A 107*, 43−52.
37. Bernacchi, S., and Mély, Y. (2001) Exciton interaction in molecular beacons: a sensitive sensor for short range modifications of the nucleic acid structure, *Nucleic Acids Res. 29*, e62.
38. Johansson, M., Fidder, H., Dick, D., and Cook, R. (2002) Intramolecular dimers: a new strategy to fluorescence quenching in dual-labeled oligonucleotide probes, *J. Am. Chem. Soc. 124*, 6950−6956.
39. Packard, B., Toptygin, D., Komoriya, A., and Brand, L. (1997) Design of profluorescent protease substrates guided by exciton theory, *Methods Enzymol. 278*, 15−23.

BI061959N